Modelling of Neutralisation of MeV Energy Protons by Impurity Ions in JET

A Stuart[1], A A Korotkov[2], A Gondhalekar, S Corti.

JET Joint Undertaking, Abingdon, Oxon, OX14 3EA.
[1] University of Cambridge, Cambridge, UK.
[2] AF Ioffe Institute, St Petersburg, Russia.

Modelling of Neutralisation of MeV Energy Protons by Impurity Ions in JET

A Stuart[1], A A Korotkov[2], A Gondhalekar, S Corti.
JET Joint Undertaking, Abingdon, Oxfordshire, OX14 3EA, UK.
[1] University of Cambridge, Cambridge, UK.
[2] A F Ioffe Institute, St. Petersburg, Russia.

ABSTRACT

A high energy neutral particle analyser was deployed on JET for measurement of the distribution function of MeV energy ICRF driven hydrogen minority ions. Unexpectedly, efficient neutralization of MeV energy protons from the plasma centre was observed without recourse to injection of atomic beams. The model developed elucidates the role of carbon and beryllium the main impurities in JET, in this process and establishes charge transfer between hydrogen-like impurity ions and protons as the major neutralization process. Uncertainties of the cross-sections and their influence on the inferred hydrogen minority distribution are discussed. Using these results, the experimental procedure in JET allows deduction of neutral deuterium density at the plasma centre.

1. EXPERIMENTAL SETUP AND OBSERVATION OF "PASSIVE" AND "ACTIVE" HYDROGEN FLUXES DURING D(H) ICRF HEATING

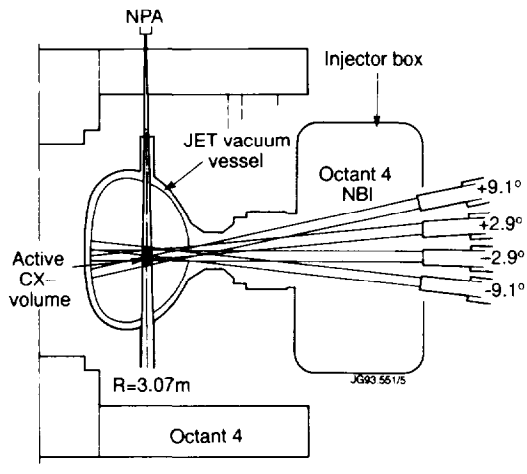

Fig.1a: Elevation of octant 4 showing vertical line of sight of NPA and neutral beam injectors.

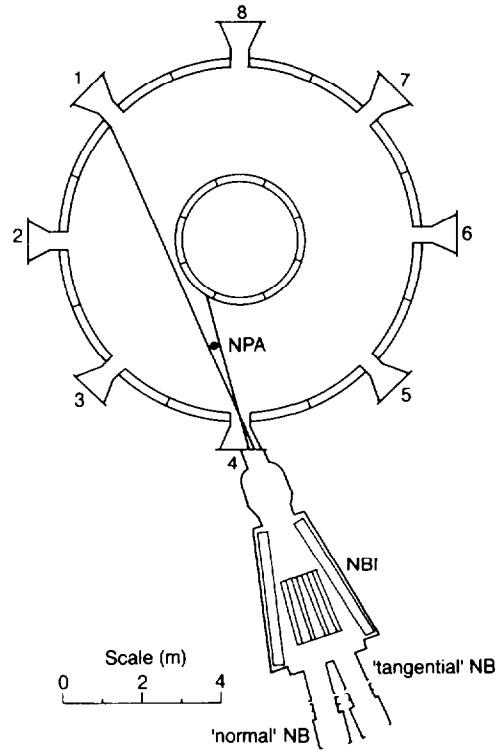

Fig.1b: Plan of torus showing position of NPA and directions of normal and tangential neutral beams.

The NPA is of the conventional EIIB type, with eight energy channels with common mass selection, capable of time resolved measurement of spectra of H, D, T, ^{3}He and ^{4}He atomic flux emitted by the plasma, in the energy range $0.3 \leq E(MeV) \leq 3.5$ [1]. The NPA was installed at the top of the torus at octant 4 with its vertical line-of-sight intersecting the plasma centre at major radius R = 3.07 m. Fig.1 shows the experimental setup.

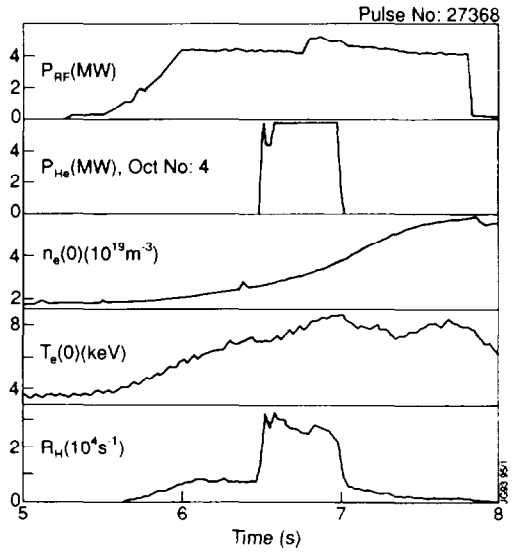

Fig.2: Evolution of plasma parameters, additional heating power and NPA count rate for channel 3.

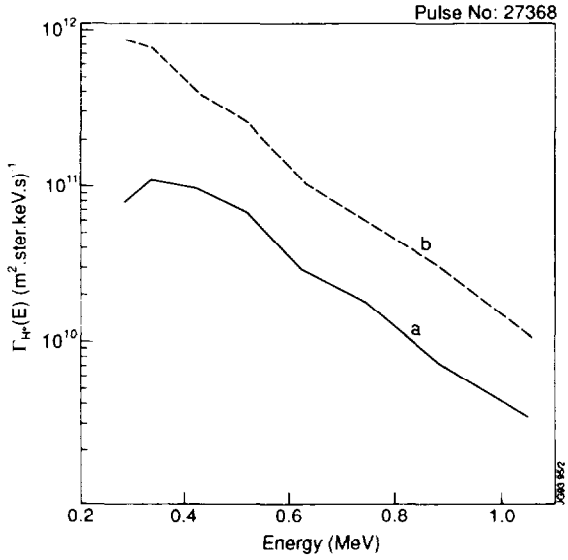

Fig.3: Energy spectrum of the flux of neutral hydrogen showing a) passive flux t = 6.4s, and b) active flux t = 6.6s.

In a typical heating experiment, a deuterium plasma with I_ϕ = 3.5 MA, B_ϕ = 2.8 T, and $\bar{n}_e = 1.9 \times 10^{19}$ m^{-3} was heated with ≅ 5 MW ICRF power for hydrogen minority heating, ≅ 5 MW of 120 kV ^{4}He^o atoms injected from oct. 4, and ≅ 5 MW of 130 kV D^o atoms injected from oct. 8. The NPA line-of-sight intersected the injected He atom beam from oct. 4 and the ICRF heating profile peaked near the plasma centre. Fig. 2 shows evolution of applied powers, $n_e(0)$, $T_e(0)$ and the count rate R_H for 0.42 MeV H^o flux received by the NPA. The expectation was that a measurable flux of neutralized ICRF driven protrons would arise only with the aid of injected atomic beams from oct. 4. Notice however that the high energy hydrogen flux detected by the NPA arose soon after ICRF power was applied and independently of the oct. 4 atom beam. We call this the "passive" flux. The "active" flux, arising only when the oct. 4 beam and ICRF were applied together is also clearly seen. The energy distribution of the H^o flux, $\Gamma_H(E)$, is shown in fig.3, for the passive flux at 6.4s and active flux at 6.6s. The uniform increase in the active flux by a factor ≈ 3.5 suggests that the injection of atoms amplifies the process giving rise to the passive flux which we take to be charge exchange (CX) between [H] impurity ions and protons. We attribute the change in the spectrum at low energy to direct CX with injected He^0. Fig. 4 shows the orbit of a 0.5 MeV proton with $v_\phi/v_z = 5 \times 10^{-3}$, the maximum permitted by the beam-line geometry. The turning point of the banana orbit is specified to be

within the NPA line of sight and the ICRF power deposition region of vertical extent $\Delta Z = \pm 0.2$ m. From such calculations we conclude that the observed hydrogen flux arises from the central regions of the plasma.

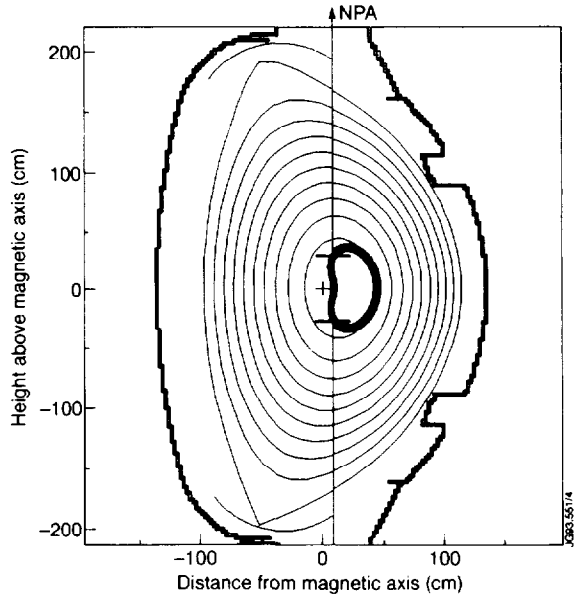

Fig.4: Poloidal projection of orbit of 0.5 MeV proton.

2. SIMPLIFIED MODEL OF IMPURITY CHARGE STATE EQUILIBRIUM

We consider a steady state plasma and treat the effects of transport of impurity nuclei by div $\Gamma_z = n_z/\tau_z$. This defines an impurity confinement time and parametrises the equation. The role of CX as a recombination mechanism in high temperature plasmas has been previously noted [2]. In the plasma centre where $\tau_z \approx 1$ s and the ion temperature is high, $T_i > 5$ keV, CX between neutral deuterium and impurity nuclei becomes the predominant recombination mechanism in spite of the low neutral density $n_o \approx 10^{-6}\, n_e$. We shall only consider [H] ions as the electron donors here since the ratio of [H] to [He] ion densities is large: 10-30 for usual JET parameters with $10^{12} < n_o\ (m^{-3}) < 10^{13}$, and reaching 50 during NBI. The density of the main donors n_{z-1} can be determined from a simple ion balance equation between nuclei and [H] ions:

$$I_{z-1} n_e n_{z-1} = n_z \left\{ \frac{1}{\tau_z} + \alpha_z n_e + \beta_z n_o + \left[\langle \sigma v \rangle^b_{cx} n_b \gamma_b + \beta_z n_h \gamma_h \right]_{oct.4} + \left[\langle \sigma v \rangle^b_{cx} n_b \gamma_b + \beta_z n_h \gamma_h \right]_{oct.8} \right\} \qquad (1)$$

where α_z is rate coefficient for radiative recombination of nuclei, β_z is rate coefficient for charge exchange with thermal neutrals, $\langle \sigma v \rangle^b_{cx}$ rate coefficient for charge exchange between nuclei and beam atoms, I_{z-1} ionization rate coefficent for [H] ions and $n_{e,o,b,h}$ are electron, majority species atom, beam and halo densities respectively. The density of impurity nuclei, n_z, is measured at the plasma centre by CX

recombination spectroscopy (CXRS) [3]. Eq.1 contains contributions from beam and halo atoms in octants 4 and 8. Oct. 8 is included since there is a possibility for [H] ions to travel halfway around the torus without ionization. Coupling of the ionization balance betweeen octants 4 and 8 during beam injection is described in eq.1 by the factors $\gamma_{b,h}$, where

$$(\gamma_{b,h})_{oct.4} = \left(1 - \exp\left[-\frac{\Delta l_{b,h}}{v_T \tau_i}\right]\right) \Big/ \left(1 - \exp\left[-\frac{2\pi R}{v_T \tau_i}\right]\right) \tag{2}$$

$$(\gamma_{b,h})_{oct.8} = \exp\left(-\frac{\pi R}{v_T \tau_i}\right) \cdot (\gamma_{b,h})_{oct.4} \tag{3}$$

$\Delta l_{b(h)}$ is the beam (halo) dimension in the toroidal direction, v_T is the average thermal velocity of the impurity ions, τ_i the ionization time and R the torus major radius.

When $\tau_i << \frac{\Delta l_{b,h}}{v_T} << \frac{\pi R}{v_T}$ [H] impurity ions created in oct. 4 do not escape from source range, $(\gamma_{b,h})_{oct.4} = 1$ and ions created in oct. 8 cannot reach oct. 4, $(\gamma_{b,h})_{oct.8} = 0$. In the opposite case $\tau_i > \frac{\pi R}{v_T}$ (full octant coupling) we obtain geometric factors $\gamma_{b,h} = \frac{\Delta l_{b,h}}{2\pi R}$ and position of beam injection is unimportant for producing the active flux.

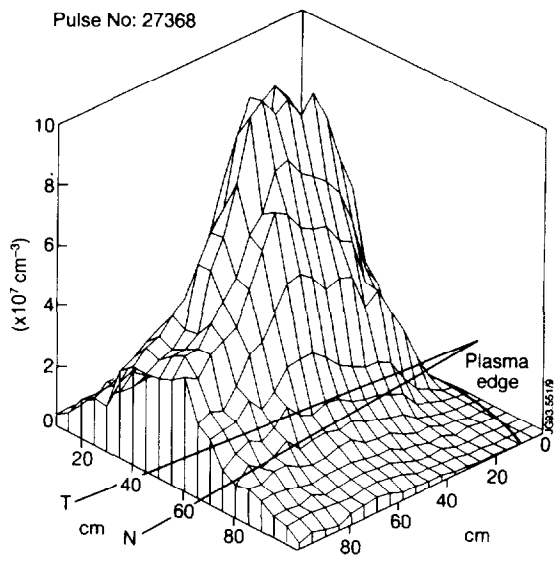

Fig.5: Typical halo distribution in the horizontal plane showing approximate positions of normal and tangential beams.

The rate coefficients used in eq.1 are known to within 10-20% because of the simplicity of the atomic systems considered. Post hoc studies contrasting our model for ionization balance with a collisional-radiative model give results consistent with errors associated with rate coefficients used. A three-dimensional Monte Carlo code has been developed to calculate the deuterium and helium halo density distribution in the plasma due to injected beams. A typical distribution of deuterium halo is shown in Fig.5. The halo density in the plasma centre under typical conditions is comparable with n_0 but because of localization of the source gives a much smaller contribution than thermal deuterium in the creation of [H] impurity ions (typically lower than 5%, but may be as large as 30% for average plasma density 6 x 10^{19} m-3).

Fig. 6 shows evolution of relevant impurity ion stages and He^0 in the NPA observation volume. Fig. 7 gives the contributions to the neutralization probability from competing processes confirming the importance of neutralization by [H] ions.

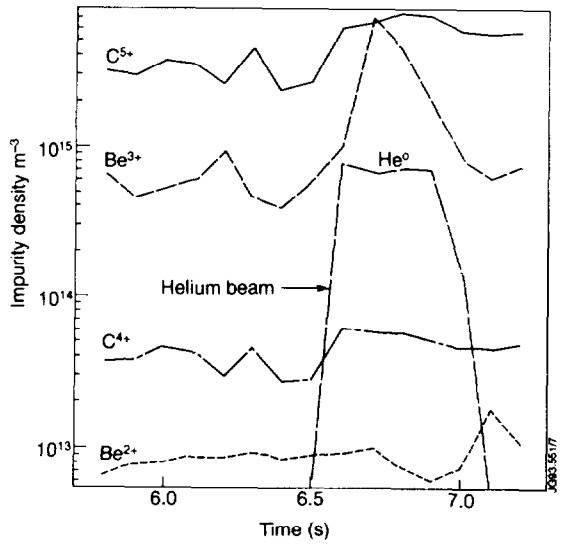

Fig.6: Evolution of ambient C^{5+}, C^{4+}, Be^{3+}, Be^{2+} and injected He^{o} densities in active CX volume.

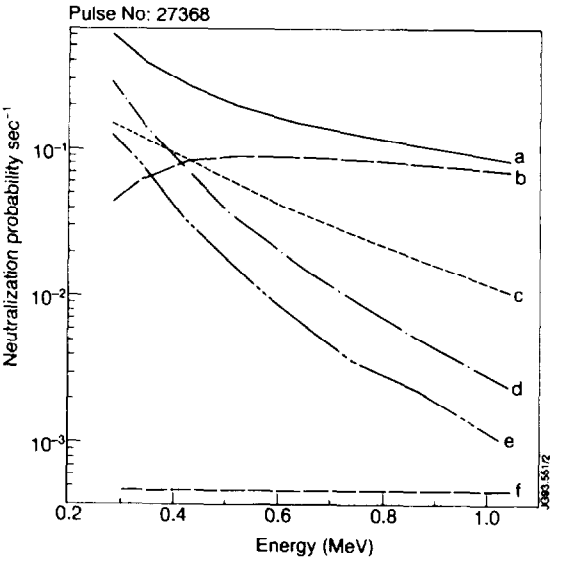

Fig.7: Probability of competing neutralization processes at t = 6.6 s. a) total neutralization rate b) p + (C^{5+},C^{4+}) ; c) p + (Be^{3+},Be^{2+}) ; d) p + (He^{+},He^{o}) ; e) p + He beam ; f) radiative recombination.

3. DETERMINATION OF NEUTRAL DENSITY AT THE PLASMA CENTRE AND HYDROGEN MINORITY TAIL TEMPERATURE

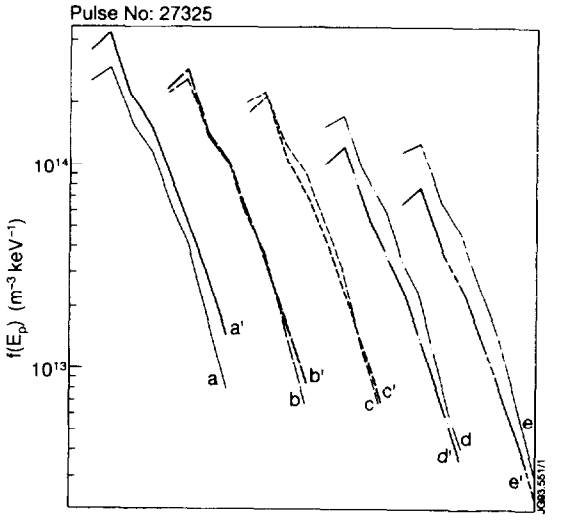

Fig.8: Variation of distribution function with n_o assuming an istotropic Maxwellian distribution for the protons. n_o (m-3) varies a) 5 x 10^{12} ; b) 1.0 x 10^{13} ; c) 1.5 x 10^{13} ; d) 3.0 x 10^{13} ; e) 5.0 x 10^{13}.

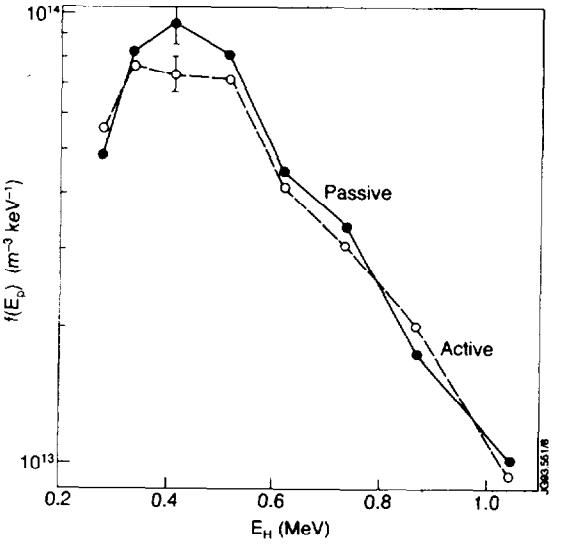

Fig.9: Inferred distribution functions from model with n_o varied to give best match.

Γ_H is proportional to the [H] ion density which in turn is highly sensitive to n_o. By comparing fluxes at two time points over a controlled change in neutral density (e.g. applying known NBI power) we can deduce the thermal deuterium density by matching the distribution functions derived from the fluxes. This procedure to determine the thermal neutral density is a new diagnostic application. Fig. 8 shows the variation of the inferred proton distribution functions with n_o. Fig. 9 shows the best match between the proton distribution functions deduced thus, obtained with $n_o = 10^{13}$ m^{-3}. The effective temperature of the proton tail distribution is deduced, T_p = 290 keV.

4. REQUIREMENT FOR ACCURATE CHARGE TRANSFER CROSS-SECTIONS, σ_{cx}, AT HIGH ENERGY

It can be shown that the uncertainty in tail temperature T_p is related to uncertainty in cross-sections by

$$\frac{\Delta T_p}{T_p} = \left[T_p \left(-\frac{d}{dE} \ln \sigma_{cx}(E) \right) \right] . \frac{\Delta \sigma_{cx}}{\sigma_{cx}} \qquad (4)$$

Fig.10 shows that to obtain good accuracy for T_p high quality atomic cross-sectional data is required. Existing data [4-7] show a 30-50% variation over the range of interest which is not acceptable for T_p >500 keV. For $100 < T_p\,(\text{keV}) < 300$ accuracy of the cross-section must be 50% for C^{5+} and 20% for Be^{3+} which is close to existing uncertainties.

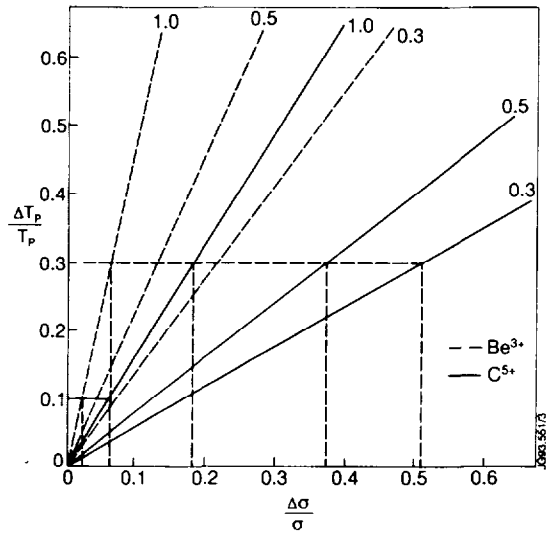

Fig.10: Dependence of errors in inferred proton tail temperature due to errors in atomic data.

Formal, perturbative solutions to the scattering amplitude give good accuracy in the asymptotic regime ($v_{proton} >> Z_{target}$) where the dominant contribution to the cross-section comes from the double scattering term [8]. Convergence to this term is not guaranteed at energies pertinent to JET. Close coupling (CC) calculations with basis states centred around the projectile and target nuclei give excellent agreement with experimental data near the peak of the cross-section. The formalism is exact provided continuum states are adequately taken into account although there is no algorithmic procedure for determination of the basis sets nor is there an internal criterion for convergence of the cross-sections with increasing number of basis states. Computational expense has precluded thorough investigations of state-to-state charge transfer cross-sections in the energy range of interest.

Utilisation of the properties of the two types of solution has been performed for $p + He^0$ [9]. We propose to extend the CC method with linear combinations of Slater-type orbitals as the basis states [10] to higher energies. These calculations will be matched to the second Born approximation in the high energy region.

REFERENCES

[1] Izvozchikov, A et al. JET-R (1991) 12.

[2] Afrosimov, V et al. JETP Letters 28 (1978) 500.

[3] Boileau, A et al. Nuclear Fusion 29 (1989) 1449.

[4] Winter, T. Phys.Rev. A35, (1987) 3799.

[5] Mukherjee and Sil. J.Phys. B13, (1980) 3421.

[6] Grozdanov and Krstic . Phys.Scripta 38, (1988) 32.

[7] Macek, J and Alston, S. Phys.Rev. A26, (1981) 250.

[8] Shakeshaft, R and Spruch, L. Rev.Mod.Phys. 51, (1979) 369.

[9] Winter, T and Alston, S. Phys.Rev. A45, (1992) 1562.

[10] Ermolaev, A. J.Phys. B17, (1984) 1069.